15th World Congress on Computational Mechanics (WCCM-XV)
8th Asian Pacific Congress on Computational Mechanics (APCOM-VIII)
Virtual Congress: 31 July – 5 August 2022
S. Koshizuka (Ed.)

NUMERICAL STUDY ON THE HYDRATE RICH SEDIMENT BEHAVIOR DURING DEPRESSURIZATION

Sahil Wani [1*], Rahul Samala[2], Ramesh Kannan Kandasami[3] and Abhijit Chaudhuri[4]

[1] Department of Civil Engineering, Indian Institute of Technology Madras
Chennai, INDIA, 600 036
*ce20d750@smail.iitm.ac.in

[2] Department of Applied Mechanics, Indian Institute of Technology Madras
Chennai, INDIA, 600 036
rsamala2@gmail.com

[3] Department of Civil Engineering, Indian Institute of Technology Madras
Chennai, INDIA, 600 036
rameshkk@civil.iitm.ac.in

[4] Department of Applied Mechanics, Indian Institute of Technology Madras
Chennai, INDIA, 600 036
abhijit.chaudhuri@iitm.ac.in

Key words: Gas extraction, depressurization, multiphase flow, THMC

Abstract. *Exploratory studies have been carried out to identify the potential natural gas hydrate reserves for commercially producing gas. While extracting the gas from the hydrate-bearing sediments using various dissociation techniques, there will be a significant loss of strength in these sediments. It is well known that the behavior of gas hydrate sediments is governed by Thermo Hydro Mechanical Chemical – THMC coupled process during the gas extraction. Thus, in this study, in order to understand the influence of depressurization at the well-bore and the permeability of the hydrate reservoir on the sediment deformation characteristics, a 2D (plane strain condition) hydrate reservoir is simulated (using a multiphase numerical schema). From the study, it is observed that the flow response, i.e., the rate of change of gas pressure near the well-bore, decreases with the increase in the duration of the extraction. The maximum settlement occurs for reservoirs having low well-bore pressure (higher amount of depressurization) and high intrinsic permeability. Additionally, these same reservoir conditions also lead to maximum cumulative gas production. Thus, the continuous gas extraction results in a highly porous medium that is stabilized primarily due to the geomechanical changes.*

1 INTRODUCTION

The unconventional source of energy in the form of gas hydrates is available in abundance throughout the world. It is roughly estimated that total gas hydrate reserves are in the range of 2831 to 85×10^5 trillion m^3 [1]. These gas hydrates are considered one of the cleaner alternatives compared to a conventional source of energy (coal). Methane gas hydrate sediments are the complex crystalline structures formed by the intrusion of the methane gas inside the lattice structure of ice [2, 3]. Methane gas hydrates are formed under suitable thermodynamic conditions, i.e., high pressure - low temperature, and are generally

found near permafrost regions or deep-sea continental shelves. Typically, these hydrate sediments are located near the continental margins at water depths between 350 and 5000 m [4]. Extracting the gas by depressurization from hydrate reservoirs reduces the pore pressure and dissociation of the methane hydrate. Due to the extraction process and the associated pressure changes, the deformation of the geo-material matrix leads to the settlement of seafloor, which might cause sub-sea landslides [5]. Hence, a critical understanding of the geomechanical response of hydrate-bearing sediments is crucial before the actual extraction of the gas from hydrate sediments.

The methane gas is extracted from hydrate when it enters an unstable pressure-temperature condition, resulting in the dissociation of hydrates into gas and water. There are various methods to extract the gas from hydrate sediments, such as depressurization [6], heating the reservoir at constant pressure (thermal injection) [6], and injection of CO_2 in the hydrate reservoir in-order to replace the methane molecules with CO_2 [7] etc. The most common methods employed are depressurization and thermal injection. In the depressurization method, the pressure in the well-bore is reduced below the phase equilibrium pressure, resulting in the dissociation of hydrates in the reservoir. With the decrease in the gas pressure, there is an increase in the overall effective stress of the gas hydrate sediments, which further leads to the deformation (settlement) near the well-bore, which is also reflected at the top of the seafloor.

The extent of depressurization at the well-bore and the intrinsic permeability of the gas hydrate reservoir greatly influences the settlement of the seafloor. With the increase in the number of vertical well-bores and hence the extraction locations, there is an increase in the subsidence of the seafloor [8]. It is reported that the settlement profile at the top of the seafloor is different when multiple well-bores are placed in the methane hydrate reservoir [8]. Jin et al. [8] concluded that subsidence of seafloor is dependent on the spacing of the well-bore (due to the change in pore-pressure variation with the number and spacing of the well-bore). Singh et al. [9] carried out a numerical investigation on gas production and settlement (using a semi-analytical model) when the reservoir is under confined and unconfined conditions in addition to the presence of mud layers. It was reported that a confined reservoir has greater settlement under the same depressurization. Further, Li et al. [10] also performed a numerical study to understand the influence of depressurization on horizontal and vertical well-bores. For the vertical well-bore, the settlements are mainly around the wellhead. However, for the horizontal well-bore, the upper layers of the soil strata also subside with the settlement around the well-bore.

In this study, the effect of depressurization of the hydrate reservoirs on the overall subsidence of seafloor and the cumulative gas production will be delineated using an in-house custom-built numerical schema. Further, a parametric study is carried out to understand the influence of intrinsic permeability on settlement characteristics and gas production.

2 THERMO HYDRO MECHANICAL CHEMICAL MODEL

2.1 Mathematical formulation

The physical phenomenon that occurs during gas extraction due to depressurization of hydrate sediments are the transmission of pressure reduction from the well-bore into the domain, the difference in pressure from equilibrium acting as driving force for hydrate dissociation, the reduction of temperature due to endothermic hydrate dissociation, the multiphase flow and heat transfer due to pressure/ temperature gradients, and the change in strength of hydrate bearing media due to reduction of hydrate saturation. The governing equations describing these thermo-hydro-mechanical-chemical (THMC) coupled processes are:

Mass balance equation for phase α*:*

$$\frac{\partial}{\partial t}\left(\phi\rho_\alpha S_\alpha\right)+\nabla\cdot\left(\phi\rho_\alpha S_\alpha \mathbf{v}_{\alpha,t}\right)=\dot{g}_\alpha+\dot{q}_\alpha, \tag{1}$$

Energy balance equation:

$$\frac{\partial}{\partial t}\left((1-\phi)\,\rho_s U_s+\sum_\alpha\left(\phi\rho_\alpha S_\alpha U_\alpha\right)\right)+\sum_\alpha\nabla\cdot\left(\phi\rho_\alpha S_\alpha \mathbf{v}_{\alpha,t}H_\alpha\right)=\nabla\cdot\left(\lambda_{eff}\nabla T\right)+\dot{Q}^h+\sum_\alpha\left(\dot{q}_\alpha H_\alpha\right) \tag{2}$$

Mass balance equation for soil phase:

$$\frac{\partial}{\partial t}\left(\left(1-\phi\right)\rho_s\right)+\nabla\cdot\left(\left(1-\phi\right)\rho_s\mathbf{v}_s\right)=0 \tag{3}$$

Stress equilibrium equation:

$$\left.\begin{aligned}\nabla\cdot\sigma+\rho_{sh}\mathbf{g}&=0\\ \sigma&=\sigma'-\alpha_b p_p\mathbf{I}\end{aligned}\right\} \tag{4}$$

The subscript $\alpha = w, g$, and h which corresponds to water, gas, and hydrate, respectively. The symbols ρ_α, S_α denote density and saturation of phase α. $\dot{g}_\alpha$ and $\dot{q}_\alpha$ represent the mass rate of phase α produced or consumed due to phase change and the mass rate of injection/production of phase α through injection/production wells. The symbols ϕ, s, U_α, H_α, λ_{eff}, T, $\dot{Q}^h$ represent the porosity, soil phase, internal energy and enthalpy of α phase, effective thermal conductivity, temperature and heat of reaction due to hydrate dissociation respectively. σ, σ' and $\mathbf{g}$ denote the total stress tensor, effective stress tensor and gravity. The notations $\rho_{sh}, \beta_{sh}, \alpha_b$ represent the density, thermal diffusivity of the combined solid and hydrate, and the biot coefficient of the solid. The pore pressure, p_p, is calculated as the saturation weighted average of gas and water pressures. $\mathbf{v}_{\alpha,t}$ denotes the total velocity of the α phase. It is related to the Darcy flux ($\mathbf{v}_\alpha$, which is relative to the solid skeleton) and the velocity of solid ($\mathbf{v}_s$) as follows:

$$\left.\begin{aligned}\phi S_\alpha\mathbf{v}_{\alpha,t}&=\mathbf{v}_\alpha+\phi S_\alpha\mathbf{v}_s\\ \mathbf{v}_\alpha&=-\tfrac{kk_{r,\alpha}}{\mu_\alpha}\left(\nabla p_\alpha-\rho_\alpha\mathbf{g}\right)\\ \mathbf{v}_s&=\tfrac{\partial\mathbf{u}}{\partial t}\end{aligned}\right\} \tag{5}$$

The symbols k, $k_{r,\alpha}$, μ_α, represent the permeability, relative permeability and viscosity of phase α. $p_\alpha, \mathbf{u}$, represent the pressure of α phase and the displacement vector respectively. Apart from the above equations, the pressures and saturations follow the closure relationships as given below.

$$\left.\begin{aligned}p_g-p_w&=p_c\\ \textstyle\sum_\alpha S_\alpha&=1\end{aligned}\right\} \tag{6}$$

The symbol p_c represents the capillary pressure. The absolute permeability is a function of hydrate saturation, whereas the relative permeability and capillary pressure are functions of gas and water saturations. These relationships are taken from Hong and Pooladi Darvish [12]. The decomposition of hydrate

is modeled according to the Kim-Bishnoi kinetics equation [13], Eq. 7, which gives the mass rate of gas produced ($\dot{g}_g$). The mass rate of water produced ($\dot{g}_w$) and the mass rate of hydrate decomposed ($\dot{g}_h$) are calculated based on the molar masses (M_w, M_g, M_h) and the hydration number, N_h (which is the ratio of the number of water molecules to methane molecules). The heat of hydrate dissociation (Eq. 7) is calculated based on the relation given by Kamath and Holder [11].

$$\left.\begin{aligned} \dot{g}_g &= k_d M_g A_{dec} (f_e - f_g) \\ \dot{g}_w &= \dot{g}_g N_h \tfrac{M_w}{M_g} \\ \dot{g}_h &= -\dot{g}_g \tfrac{M_h}{M_g} \\ \dot{Q}_h &= \tfrac{\dot{g}_h}{M_h} (c + d \cdot T) \end{aligned}\right\} \tag{7}$$

A_{dec} denotes specific surface area of hydrate decomposition [14]. k_d is the kinetic rate constant, and f_e and f_g are the fugacities of methane at equilibrium condition and gas phase, respectively. The fugacities and density of gas are calculated using the Peng-Robinson equation of state. The parameters c and d are from Kamath and Holder [11]. The relation gives the kinetic rate constant k_d:

$$k_d = k_d^o exp\left(-\frac{E}{RT}\right) \tag{8}$$

where k_d^o is the intrinsic rate constant, E is the activation energy, R is the universal gas constant. The hydrate equilibrium conditions (p, T) are calculated using the correlation of Kamath and Holder [11],

$$p = \exp\left(38.98 - \frac{8533.8}{T}\right); \quad p \text{ in kPa and } T \text{ in K} \tag{9}$$

Different constitutive models are available in literature [3] for gas hydrate sediments. For this study, the simple elastic model was adopted, including the dependence of shear modulus on hydrate saturation. The constitutive relationship used in the model has represented in Eq. 10. The constitutive stiffness matrix is dependent on the bulk modulus (K) and shear modulus (G). The bulk modulus in hydrate sediments is contributed by soil skeleton and hydrate. It is assumed that the bulk modulus of soil skeleton dominates the overall bulk modulus of hydrate-bearing sediment [15]. The shear modulus of hydrate sediments increases due to the presence of hydrates in the voids, resulting in the enhancement of the shear modulus. The relationship between bulk modulus (K) and shear modulus (G) is taken from Uchida et al. [15]. The symbols $\mathbf{D}$, σ', and ε in Eq.10 represent the constitutive stiffness matrix, effective stress tensor and strain tensor.

$$\left.\begin{aligned} \sigma' &= \mathbf{D}\varepsilon \\ \mathbf{D} &= \begin{bmatrix} K+\frac{4}{3}G & K-\frac{2}{3}G & K-\frac{2}{3}G & 0 & 0 & 0 \\ K-\frac{2}{3}G & K+\frac{4}{3}G & K-\frac{2}{3}G & 0 & 0 & 0 \\ K-\frac{2}{3}G & K-\frac{2}{3}G & K+\frac{4}{3}G & 0 & 0 & 0 \\ 0 & 0 & 0 & G & 0 & 0 \\ 0 & 0 & 0 & 0 & G & 0 \\ 0 & 0 & 0 & 0 & 0 & G \end{bmatrix} \end{aligned}\right\} \tag{10}$$

2.2 Implementation

A numerical simulator to solve the THMC coupled equations describing the hydrate phase change kinetics, non-isothermal multiphase flow in porous media, and geomechanics is developed. The multiphase flow and heat transfer equations are discretized using the finite volume method (FVM), and the stress equilibrium equation is discretized using the finite element method (FEM). Newton's method is used to linearize the non-linear algebraic equations, and the linearized equations are solved in a fully implicit simultaneous procedure. A minimum residual method is used to solve the linear equations iteratively. In the present work, PETSc routines, developed by Argonne National Lab USA, have been used. The Newton's line search non-linear solver and GMRES linear solver of PETSc are used to solve the discretized equations.

3 NUMERICAL MODEL FOR THE STUDY

The domain and numerical grid used for simulations of dissociation of hydrate-bearing sediments are discussed in this section. A homogeneous hydrate reservoir of a height of 30 m located at 1200 m below sea level and 200 m below the seafloor was considered for this study. A well-bore of height 4 m was placed at the bottom of the domain (Fig. 1). The temperature at the top of the hydrate reservoir was considered to be 283.15 K, and it increased with depth at a rate of 0.03 K/m. The initial pore pressure at the top of the domain was about 12 MPa. The length of the domain was fixed after performing a domain convergence test. The bottom of the domain was vertically restrained, and the extreme left side was laterally restrained for the numerical simulations. All sides were considered impervious (no flow condition) except the nodes at the well-bore. The hydraulic properties of the reservoir are given in Table 1.

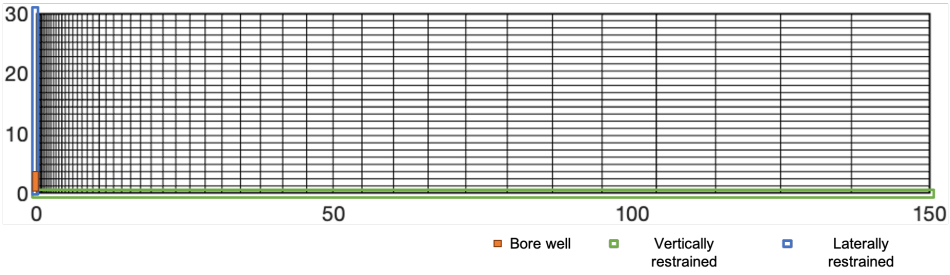

Figure 1: Final domain and mesh for the numerical study

Table 1: Properties for gas hydrate sediments

Parameters	**Value**
Porosity	0.28
Intrinsic permeability (mD)	$5, 10$
Initial Temperature (K)	283.15
Initial Hydrate Saturation	0.6
Well-bore Pressure (MPa)	$6, 3$
Thermal expansion coeff (K^{-1})	$\beta_s = 18 \times 10^{-6}; \beta_w = 2.1 \times 10^{-4}; \beta_h = 2.6 \times 10^{-4}$
Specific heat (J/kg.K)	$C_{ps} = 800; C_{ph} = 1600; C_{pg} = 2162; C_{pw} = 4179$
Thermal conductivity (Wm.K)	$\lambda_s = 1.5; \lambda_h = 0.393; \lambda_g = 0.0033; \lambda_w = 0.6$

3.1 Selection of domain and mesh

The hydrate reservoir is semi-infinite in the field, and it will be computationally expensive to simulate the entire length. In order to determine the critical length of the domain (x), beyond which there is a negligible effect of the length of the domain on the numerical results, a domain convergence study was performed. The domain lengths of 25 m, 50 m, 100 m, 150 m, 200 m, and 300 m were considered for this study. It was observed from the Figure 2a that beyond the 150 m, there was no significant change in the vertical displacement (at three different locations after one month). The difference in the displacement at the top of the domain for the 150 m and 300 m domain was 0.104%, and for the other two locations, it was even less than 0.1%.

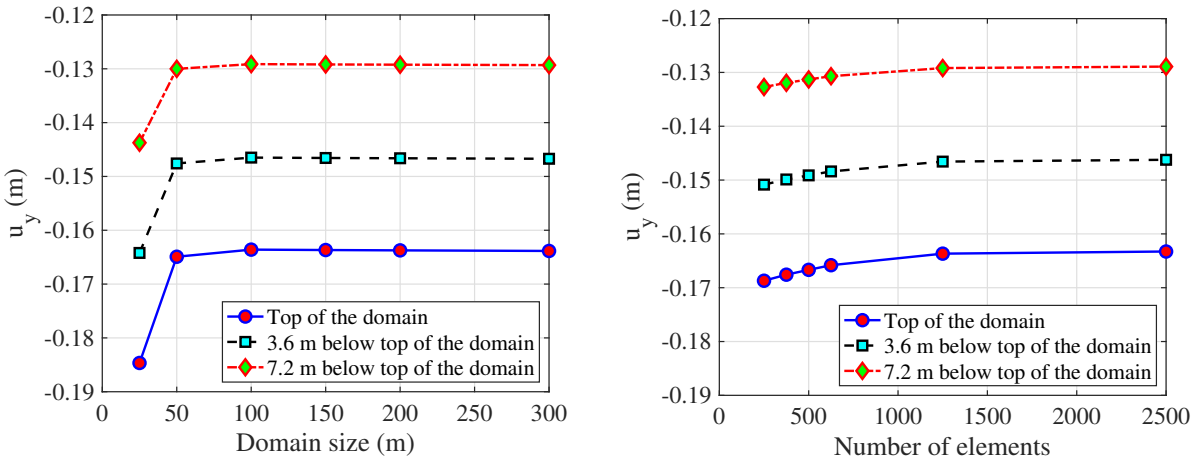

Figure 2: Vertical displacement for left edge element (in vertical line of well-bore) (a) Domain convergence (b) Mesh convergence

In general, the usage of finer numerical grid size generates more accurate results. However, the number of elements increases with a finer numerical grid because of which the computational time increases. In order to arrive at a balance between accuracy and computational time, an optimum grid size should be

adopted. In the present study, the numerical model was simulated for the different number of elements. Figure 2b shows the variation of vertical displacement at different locations with the increasing number of elements. The difference in the vertical displacement at the top of the domain between 1250 elements and 2500 elements was 1.5%, and for the other two locations, it was even less than 1.5% (difference was less than 0.002 m). It was observed that beyond 1250 elements, there was no significant change in the vertical displacement (for all the three different locations). Hence, after the domain and mesh convergence analysis, the domain size of 30 m $\times$ 150 m with 1250 elements (the domain was discretized into 25 $\times$ 50 elements) was adopted for the further numerical study.

4 RESULTS AND DISCUSSION

The amount of depressurization achieved (the difference between formation pressure and well-bore pressure) plays a crucial role in the amount of gas extracted and also the subsidence of the seafloor. Also, the intrinsic permeability of the hydrate reservoir has a great influence on the propagation of the pore pressure wavefront in the domain, which is the main cause of the settlement. Table 2 shows the different cases simulated for this study.

Table 2: Different cases analysed for the study

Case	Intrinsic permeability	Well-bore pressure
1	5 mD	3 MPa
2	10 mD	3 MPa
3	5 mD	6 MPa
4	10 mD	6 MPa

Figure 3 represents the vertical settlement at the top of the domain (along the length of the domain) after 30 days, 90 days, and 360 days of gas production for the different cases as mentioned in Table 2. The vertical settlement decreases horizontally away from the well-bore because of less mobilization in pore pressure from the initial formation pressure. It was observed in Figure 3a that the vertical displacement at the top of the domain is maximum for case 2, followed by cases 1, 4, and 3. It was also observed that the temporal variations of the vertical settlement also follows similar order. In case the reservoir has the same permeability, a lower well-bore pressure causes greater vertical displacement. This is due to the fact that at lower well-bore pressure, there is a greater reduction in the pore pressure from its equilibrium state, which leads to an increase in the effective stress of the hydrate sediments resulting in a higher settlement. It was also observed that the vertical displacement curve along the length of the domain becomes more flatter with time for the reservoir with the higher permeability (10 mD) as compared to lower permeability (5 mD), as shown in Figure 3a to 3c. This response is obtained as a result of faster diffusion of pore pressure into the domain due to high permeability, as shown in Figure 4. During the extraction of gas, in addition to the total settlement, differential settlement also plays a crucial role. Additional shear stresses are developed due to differential settlement causing the landslide of the seafloor. Thus, it is important to have less differential settlement while extracting the gas. The differential settlement (difference in the vertical settlement at two extreme ends) along the length at 360 days was least ($\approx$ 21%) for case 4, the reservoir with the highest permeability and higher well-bore pressure. For cases 2 and 3, the differential settlement was intermediate (within the range of 41%-43%), and case 1 had the maximum differential settlement ($\approx$ 55%). The differential settlement was caused due to the

difference in the effective stress developed along the length of the domain, which in turn depends on the variation of the pore pressure, which is maximum for case 1 and minimum for case 4. The variation of pore pressure in the reservoir depends on the well-bore pressure and the reservoir's permeability. For the same reservoir permeability, the higher the amount of depressurization (i.e., lower the well-bore pressure), the greater will be the variation of pore pressure (as shown in Figure 4) along the length of the reservoir, resulting in the higher differential settlement as well as overall settlement. Similarly, for the same well-bore pressure, the lower the reservoir permeability, the slower the pore pressure dissipation into the domain. This leads to a higher variation of pore pressure in the domain, resulting in a higher differential settlement but less overall settlement (cases 1 and 3 compared to cases 2 and 4).

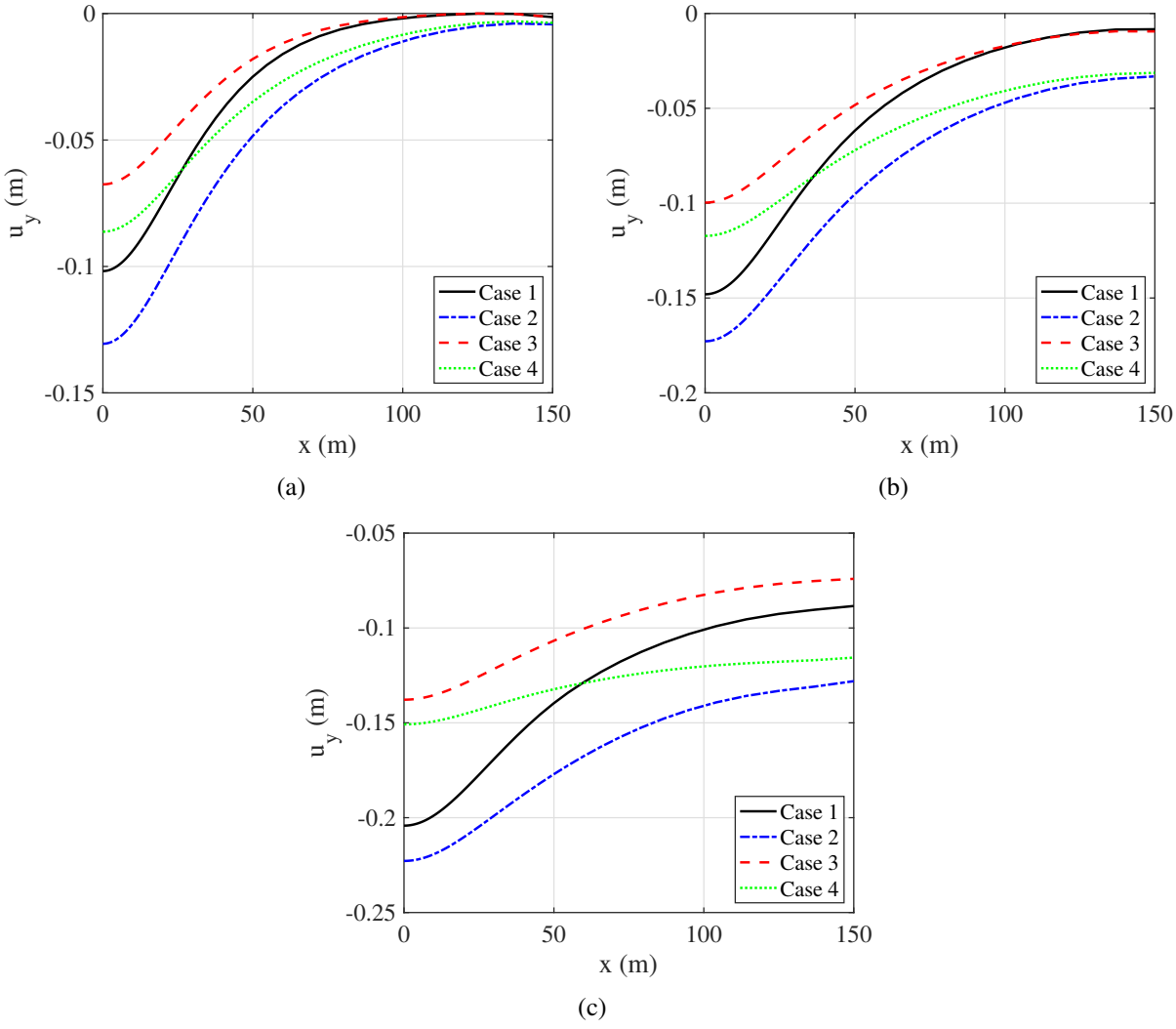

Figure 3: Vertical displacement at the top of the domain (a) 30 days (b) 90 days (c) 360 days

Figure 5a shows the variation of maximum vertical displacement at the top left corner of the domain with time. From the predictions, it can be understood that for cases 3 and 4 (higher well-bore pressure),

the vertical settlement is less than for cases 1 and 2 (lower well-bore pressure). Further, it can also be observed that the rate of settlement decreases with time for all the cases. The rate of settlement is minimum for case 3 and maximum for case 2. It was observed that for cases 3 and 4, there is not much change in the vertical settlement from day 90 to day 360 when compared to cases 1 and 2. This response can be correlated with the pore pressure variation as shown in Figures 4b and 4c, where there is not much change in pore pressure from day 90 to day 360. For cases 1 and 2, the rate at which the settlement changes is greater than for cases 3 and 4. The higher amount of depressurization in cases 1 and 2 results in the development of higher effective stresses in the hydrate sediments, thus causing the more vertical displacements, as shown in Figure 5a.

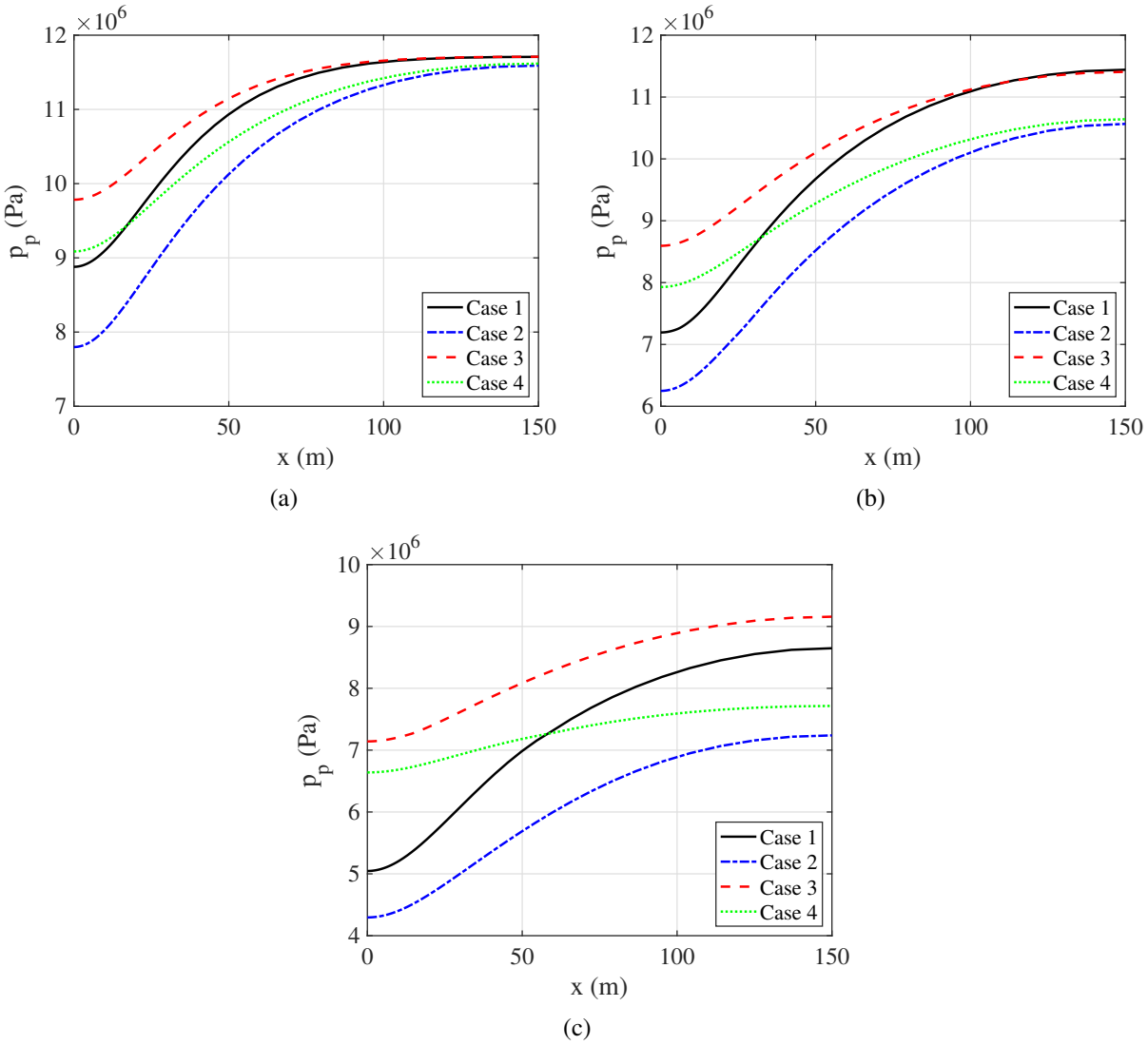

Figure 4: Pore pressure variation at the top of the domain (a) 30 days (b) 90 days (c) 360 days

Figure 5b represents the cumulative gas production (Q_{cum}) for different cases. Amongst the four cases discussed in this study, the cumulative gas production was the maximum for case 2 (high permeability and low well-bore pressure), followed by cases 1, 4, and 3. Further, the rate of increase of cumulative gas production decreases with time for all the cases. It was also observed that with a higher amount of depressurization (lower well-bore pressure), the extent of dissociation is greater, and with higher permeability, there is faster diffusion of pore pressure wavefront, leading to an increase in the rate of gas production. Hence, the higher depressurization and permeability (case 2) of the medium produces the higher cumulative gas production, while case 3 exhibits the least cumulative gas production. It was observed that case 4 has slightly higher cumulative gas production as compared to case 1 up to 100 days, beyond which case 1 has higher cumulative gas production. The well-bore pressure and intrinsic permeability have an opposing effect on the amount of gas produced. While a higher amount of depressurization due to lower well-bore pressure increases the production of gas, lower permeability restricts the diffusion of pore pressure reduction into the domain resulting in a lower amount of overall gas produced in the domain. It was also observed that initially, the intrinsic permeability dominates compared to the amount of depressurization. Hence, case 4 has higher intrinsic permeability and thus has a higher amount of pore pressure dissipation than case 1, which has slightly higher cumulative gas production even though case 1 has a higher amount of depressurization. As time progresses, the gradient of pore pressure decreases along the length into the domain, leading to a higher amount of depressurization than in case 4 when compared to case 1, thus resulting in higher cumulative gas production for case 1 as compared to case 4.

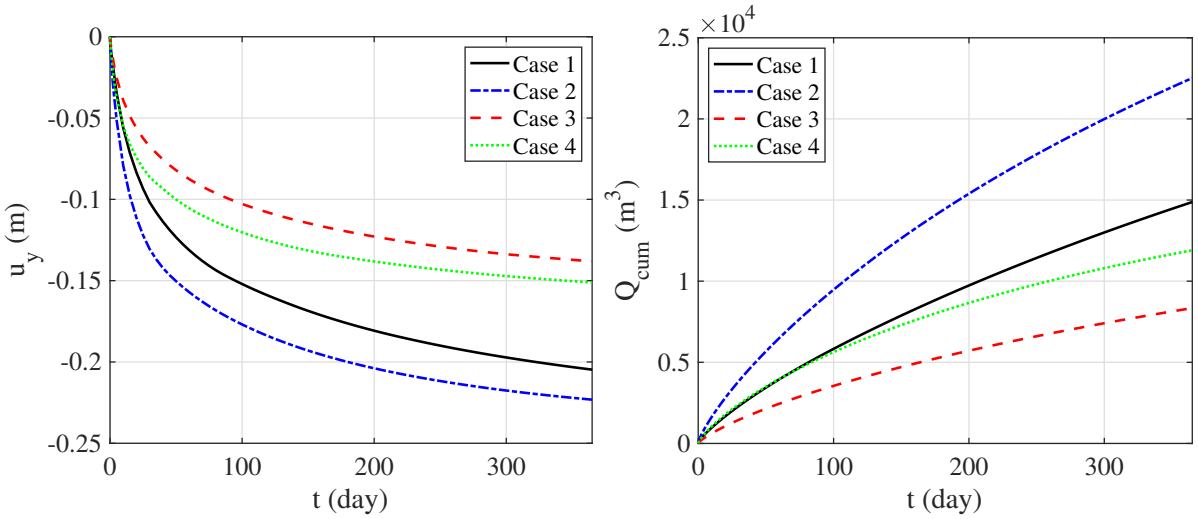

Figure 5: Variation along the time (a) Maximum vertical displacement (b) Cumulative gas production

5 CONCLUSIONS

The influence of depressurization and intrinsic permeability on the vertical displacement and cumulative gas production of a gas hydrate reservoir was studied using a coupled numerical schema. The mathematical formulation consists of mass balance equations for gas, water, and hydrate, energy balance equation, and stress equilibrium equation. The hydrate dissociation kinetics was modeled after

Kim-Bishnoi kinetics formulation. The governing mass balance and energy equations are discretized using finite volume method (FVM) while the stress equilibrium equation was discretized using finite element method (FEM). The non-linear and linear solvers of PETSc have been used to solve the discretized equations. The main conclusions obtained from this study are as follows:

- Vertical displacement at the top of the hydrate reservoir was maximum for the case with a higher amount of depressurization and higher permeability
- For the same amount of depressurization, the higher the permeability of the hydrate reservoir, the faster is the pore pressure diffusion, resulting in less differential settlement
- Under a higher amount of depressurization and higher permeability, the rate of hydrate dissociation is also higher, resulting in higher cumulative gas production

6 ACKNOWLEDGEMENTS

We gratefully acknowledge the support provided by the Department of Science and Technology, SERB – (SRG/2020/002126), INDIA for carrying out this research.

REFERENCES

[1] Mahajan, D., Taylor, C.E. and Mansoori, G.A. An introduction to natural gas hydrate/clathrate: The major organic carbon reserve of the Earth. *Journal of Petroleum Science and Engineering* (2007) **56**:1–3

[2] Hawtin, R.W., Quigley, D. and Rodger, P.M. Gas hydrate nucleation and cage formation at a water/methane interface. *Physical Chemistry Chemical Physics* (2008)**10**:4853–4864

[3] Wani, S., Samala, R., Chaudhuri, A., & Kandasami, R. K. Efficacy of elastic-plastic constitutive models in predicting the geo-mechanical response of gas hydrate sediments. *E3S Web of Conferences* EDP Sciences (2020) **205**:13012

[4] Meehl, G.A., Stocker, T.F., Collins, W.D., Friedlingstein, P., Gaye, A.T., Gregory, J.M., Kitoh, A., Knutti, R., Murphy, J.M., Noda, A. and Raper, S.C. Global climate projections. Chapter 10.(2007).

[5] Kim,J.;Moridis,G.J.;Rutqvist,J. Coupled flow and geomechanical analysis for gas production in the Prudhoe Bay Unit L-106 well Unit C gas hydrate deposit in Alaska.J. *Journal of petroleum science and engineering* (2012) **92**:143–157

[6] Zheng, R., Li, S. and Li, X. Sensitivity analysis of hydrate dissociation front conditioned to depressurization and wellbore heating. *Marine and petroleum geology* (2018)**01**:631–638

[7] Englezos, P. Extraction of methane hydrate energy by carbon dioxide injection-key challenges and a paradigm shift. *Chinese Journal of Chemical Engineering* (2019)**27**:2044–2048

[8] Jin, G., Lei, H., Xu, T., Xin, X., Yuan, Y., Xia, Y. and Juo, J. Simulated geomechanical responses to marine methane hydrate recovery using horizontal wells in the Shenhu area, South China Sea. *Marine and Petroleum Geology* (2018) **92**:424–436

[9] Singh, R.P., Yadav, R., Muralidhar, K. and Das, M.K. Effect of confined boundary and mud-layers on depressurization-based gas recovery and land subsidence in hydrate reservoirs. *Marine Georesources & Geotechnology* (2022) **40**:78–95

[10] Li, Y., Cheng, Y., Yan, C., Wang, Z., Zhang, Q. and Zhou, P. Stratum Settlement during Depressurization of Horizontal Wells in Gas Hydrate Reservoirs. *Energy & Fuels* (2021) **35**:14692–14708

[11] Kamath, V. A. and Holder, G. D. Dissociation Heat Transfer Characteristics of Methane Hydrates. *AIChE Journal* (1987) **33**:347–350

[12] Hong, H. and Pooladi Darvish, M. Simulation of Depressurization for Gas Production From Gas Hydrate Reservoirs. *J Can Pet Technol* (2005) **44**:39–46

[13] Kim, H.C., Bishnoi, P.R., Heidemann, R.A. and Rizvi, S.S. Kinetics of methane hydrate decomposition. *Chemical engineering science* (1987) **42**:1645–1653

[14] Sun, Xuefei and Mohanty, Kishore K. Kinetic simulation of methane hydrate formation and dissociation in porous media. *Chemical Engineering Science* (2006) **61**:3476–3495

[15] Uchida, S., Soga, K. and Yamamoto, K., 2012.Critical state soil constitutive model for methane hydrate soil. *Journal of geophysical research: solid earth* (2012) **117**:B3